Simulation of supersonic gas-particle flows expanding from the nozzle into rarefied atmosphere

Daniel Bodanyuk[1], Vladislav Emelyanov[1], Alexander Pustovalov[1], Konstantin Volkov[2,*]

[1]Baltic State Technical University, St Petersburg, 190005, Russia
[2]Kingston University, London, SW15 3DW, United Kingdom

Abstract

The results of numerical simulation of the particle-laden supersonic flows expanding from converging-diverging nozzle into a rarefied atmosphere are presented. To calculate flow quantities in a wide range of nozzle pressure ratios and investigate a possibility of a strong turn of the flow at the nozzle outlet, a marching scheme and finite volume method are applied. The marching calculations of the supersonic jet starts from the nozzle section, in which supersonic flow velocities are realized. The trajectories of motion of solid particles during the flow expansion are provided. The influence of the particle size and coordinates of the particle injection point into the flow on their transport by a supersonic flow is discussed. The results of calculations obtained in the framework of the Stokes approximation for the drag coefficient of an individual particle and with corrections for the inertia of the particle and rarefaction of the gas flow are compared. Conclusions are drawn about the effect of the dispersed phase on the distribution of gas flow quantities. The calculation results are of interest for studying supersonic particle-laden flows around bodies and for calculating oblique shock waves.

Keywords

flight safety, nozzle, jet, supersonic flow, Prandtl–Meyer flow, rarefaction wave, particle, two-phase flow.

1 Introduction

In space engineering, various devices are used, during the operation of which jet flows develop. These include, in particular, devices that create control forces necessary for the orientation of spacecraft. A feature of the operation of such devices is the jet expansion into a medium with low pressure and their expansion in a wide range of speeds [1]. The jets of the control system engines have a negative impact on the design of the spacecraft and the surfaces of instruments [2, 3], being one of the reasons for the deterioration of their operational characteristics. The impact of jets is reduced to force (local force loads, total perturbing forces and moments), thermal (local and total thermal loads) and physical and chemical (changes in the properties surfaces washed by jets) impacts, as well as the influence of particles on the operation of on-board equipment (optical, radio engineering) and the failure of the astro-navigation system (sunlight scattered by particles is perceived as stars).

*Corresponding author: k.volkov@kingston.ac.uk

The shape of the jet, the structure of shock waves and mixing layers, and the distribution of parameters in the jet depend on the altitude and speed of the flight. Combustion products of high-energy rocket propellants are multi-component mixtures with high stagnation temperatures. The presence of condensed particles in the combustion products leads to the formation of a two-phase flow, which develops under conditions of transition from the continuum flow regime to the rarefied flow regime [4, 5]. Particles of the condensed phase not only affect the functioning of space technology, being deposited, for example, on the elements of optical systems, but are also long-lived formations, creating a special form of pollution of the space environment [6–8].

The creation of universal methods for calculating jet flows based on the numerical solution of the full Navier–Stokes equations or the Reynolds-averaged Navier–Stokes equations is not always expedient. This is connected not so much with the problems of numerical solution of the equations themselves, but with the existing uncertainties in the values of the coefficients of the turbulence models, the kinetic parameters of combustion, and interphase interaction. When solving applied problems, it becomes necessary to formulate simplified mathematical models and develop algorithms that take into account the features of the flows.

One of the methods for modelling stationary supersonic flows is the marching method. In the case of the appearance of gas wave disturbances propagating against the flow direction, the use of marching calculation methods becomes problematic. If there are subsonic regions in the computational domain (external subsonic flow, subsonic zone behind the Mach disk), special approximations are applied to expand the range of applicability of the marching method. Suppression of upwind disturbances in subsonic flow regions is possible by making additional changes to the Navier–Stokes equations [9]. In particular, the semi-permeable boundary approximation is used, which makes it possible to limit the flow turn angle at the nozzle edge, thus preventing the formation of a subsonic region [10].

A large number of studies are devoted to the theoretical study of the expansion of an ideal perfect gas flow into a vacuum [11–13]. In particular, in [12,13] the results of numerical calculations for conical nozzles are presented in graphical and tabular form for various Mach numbers and nozzle angles. The limitations of the performed calculations for the half-opening angle are associated with an increase in computer time and calculation errors.

A numerical study of the expansion of supersonic jets into a co-current flow is carried out in [14] on the basis of the parabolized Navier–Stokes equations. To calculate the jet flowfield in [15], flow is divided into supersonic and subsonic zones, and assumes that the pressure is constant in the subsonic part of the mixing layer. The flow in the supersonic non-isobaric zone of the jet is calculated on the basis of the parabolic Navier–Stokes equations, and the flow in the subsonic part of the mixing layer is described by the equations of the boundary layer. A procedure for matching local solutions and a method for solving boundary layer equations is proposed in [16], which makes it possible to determine the position of the outer boundary of the computational domain based on local flow gradients.

Due to the presence of a boundary layer on the nozzle walls, the gas density in the peripheral part of the jet is much higher than the density calculated from the model of inviscid gas flow into vacuum. Study of [17] proposes an approximate model that makes it possible to improve the accuracy of calculating the parameters of a supersonic jet expanding into a vacuum. The area of applicability of the model is the far field of the jet, which starts from the continuity boundary and extends downstream, where the gas velocity approaches the limiting value, and the streamlines remain rectilinear.

In the works [18,19], the finite volume method and the marching method are applied to

numerical simulation of stationary supersonic flows of an ideal compressible gas in curvilinear channels and nozzles with various nozzle pressure ratios. The flow patterns in supersonic jets that arise when a uniform velocity distribution and a velocity distribution corresponding to a free vortex are realized at the nozzle outlet are compared.

As a model problem, which has the characteristic features of supersonic jets expanding into a low-pressure medium, the Prandtl–Meyer flow (flow near the expansion corner) is considered. Particle trajectories in the Prandtl–Meyer flow are calculated in [20] for various initial flow parameters, and the effect of particles on the structure of the rarefaction fan is discussed in [21, 22]. To find particle trajectories, the equations of motion are written in the polar coordinates. For simplicity, the Stokes drag law is used for particles [20]. The transition of the gas-particle flow from the equilibrium regime far from the corner to the frozen regime after the expansion of the flow is considered in [21]. The influence of particles on various flow regimes that occur during shock wave diffraction is discussed in [23]. The influence of rarefaction of the medium on the motion of particles in a jet expanding into vacuum is considered in [24].

A model of a two-phase flow, which takes into account the possibility of flow around particles at arbitrary Knudsen numbers (from the continuum to free molecular flow), was constructed in [25]. In the supersonic part of the nozzle, the particles do not have time to turn around together with the expanding gas and form a cumulated bundle, the narrower, the denser the material of the particle [26]. The optical characteristics of the compressed layer formed when a poly-dispersed jet impinges on a blunt body are studied in [27].

With the free expansion of a supersonic jet of a gas into vacuum, conditions appear for condensation and further formation of clusters [28]. Condensation of the gas with the formation of clusters occurs both in the nozzle and behind its critical section. The nozzle geometry determines the main parameters associated with the cluster size, beam intensity, beam divergence and temperature. The formation and growth of clusters in gas jets occur more efficiently with increasing stagnation pressure, decreasing stagnation temperature, and increasing nozzle diameter [29, 30].

The influence of the angle of a conical nozzle on the structure of the formed jet is studied in [31, 32]. Near the edge of the nozzle, there is a reversed flow and reversed movement of drops in the direction opposite to the direction of flow in the central part of the jet [33–35]. In the reversed flow, individual particles leaving the nozzle turn by more than 90 degrees and begin to move towards the central part of the jet [36]. Study of [37] uses a hybrid method to simulate the flow in various modes (from the flow of a continuous medium inside a nozzle to the free molecular mode in the reversed flow region), which combines the simulation of the Navier–Stokes equations with direct simulation of Monte Carlo. The reversed flow is only a small part of the total mass flow in the jet. The aerodynamic forces are not strong enough to wrap the droplets around the edge of the nozzle. The droplets present in the reversed flow the cooling film, which breaks down at the edge of the nozzle.

The expansion of a supersonic jet into a medium with low pressure is characterized by large gradients of density, velocity, pressure and temperature. Even in the case of stationary problems, these flows exhibit an extremely wide range of thermodynamic parameters, which creates difficulties for numerical methods [38, 39].

In this study, numerical simulation of supersonic jets expanding into a medium with low pressure and transport of particles by flows, the parameters of which are typical for elements of space systems, are considered. Estimates are given and questions of the influence of rarefaction of the medium on the transport of particles of the dispersed phase are discussed.

Both the features of the motion of individual particles in a centered rarefaction wave and their influence on the parameters of the carrier flow are considered. Calculations are carried out for various particle sizes and coordinates of the points of their injection into the carrier flow. The results of calculations of nozzle flows and jets expanding into a medium with low pressure are presented. The effect of corrections for the particle inertia and rarefaction of the gas flow to the drag coefficient of an individual particle on the results of numerical simulation is discussed.

2 Flow pattern

It is assumed that the gas is at rest in the nozzle reservoir, and its density is determined by the total pressure, p_0, and the total temperature, T_0. The gas expands into atmosphere with pressure p_∞. The model of inviscid compressible gas is used for calculations. The effects of viscosity and rarefaction of the gas flow are taken into account only when the gas interacts with particles.

The presence of a pressure gradient leads to gas expansion through the nozzle throat, where its velocity reaches the speed of sound, and then expands in the supersonic part of the nozzle (Figure 1). As the gas expands, the density and temperature of the gas decrease. A decrease in density also leads to a decrease in the number of inter-molecular collisions, which prevents instantaneous energy exchange between molecules and thermodynamic non-equilibrium. The rarefaction and the subsequent establishment of non-equilibrium lead to the violation of the assumption about the continuum of gas flow from the nozzle.

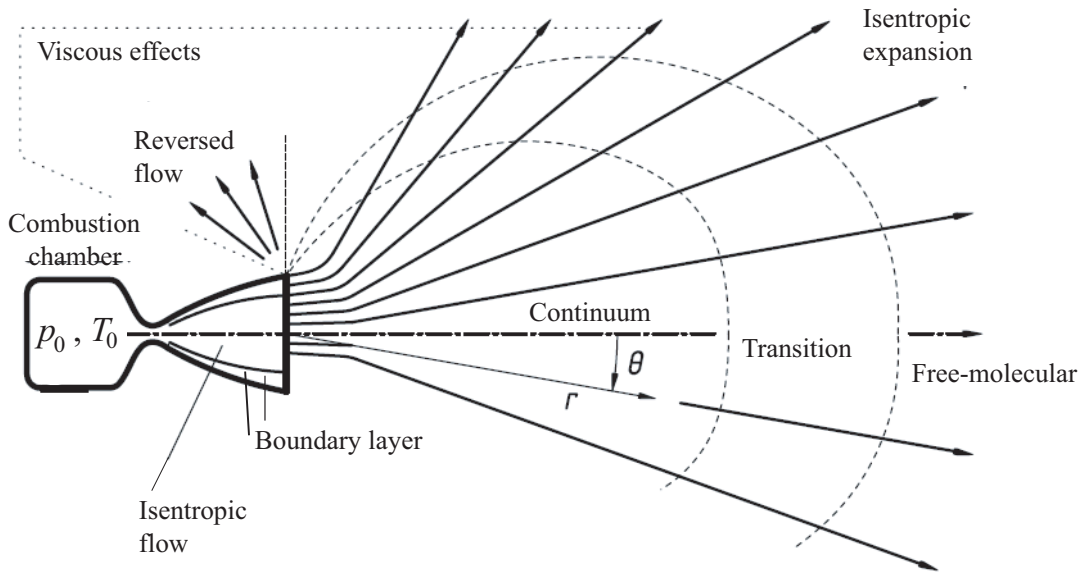

Figure 1. Scheme of jet flow from the nozzle into vacuum

The flowfield of a jet of an ideal perfect gas expanding into a vacuum, is divided into three characteristic regions. Region 1 is bounded by the nozzle outlet and the first characteristics of the AB. The flow in region 1 is a continuation of the flow in the nozzle. Region 2, bounded by the characteristics AB and the jet boundary, is a rarefaction flow. In the plane case, the Prandtl–Meyer flow occurs in region 2. Flow in the region 3 is formed

as a result of the interaction of the characteristics of the first and second families and, in the first approximation, has the character of an expansion in a supersonic source. At the boundaries of the regions, the gas-dynamic quantities remain continuous, and their normal derivatives suffer a discontinuity. The jet boundary is rectilinear both in the plane and in the axisymmetric case.

3 Mathematical model

The temperature dependence of the thermophysical properties of the particle material affects its transport by the carrier flow. A decrease in the speed of sound in the carrier gas leads to supersonic values of the relative Mach number (even at a small difference in the velocities of the gas and particles). Expansion of the carrier gas and an increase in the mean free path of molecules leads to a free molecular flow around individual particle, when a correction for the rarefaction of the flow is taken into account [4, 5].

3.1 Gas

In the two-dimensional case, the equation describing the steady-state flow of an inviscid compressible gas has the conservative form

$$\frac{\partial \boldsymbol{F}}{\partial x} + \frac{\partial \boldsymbol{G}}{\partial y} = 0. \tag{1}$$

The equation (1) is supplemented by the equation of state for a perfect gas

$$p = (\gamma - 1)\rho\varepsilon.$$

The total energy per unit volume is found from the relation

$$e = \rho\varepsilon + \frac{1}{2}\rho(u^2 + v^2).$$

The vector of conservative variables $\boldsymbol{U}$ and the flux vectors $\boldsymbol{F}$ and $\boldsymbol{G}$ have the following form

$$\boldsymbol{U} = \begin{pmatrix} \rho \\ \rho u \\ \rho v \\ e \end{pmatrix}, \quad \boldsymbol{F} = \begin{pmatrix} \rho u \\ \rho uu + p \\ \rho uv \\ (e + p)u \end{pmatrix}, \quad \boldsymbol{G} = \begin{pmatrix} \rho v \\ \rho uv \\ \rho vv + p \\ (e + p)v \end{pmatrix}.$$

Here, ρ is density; u and v are velocity components in coordinate directions x and y; p is pressure; e is total energy per unit volume; ε is specific internal energy; γ is ratio of specific heat capacities at constant pressure and constant volume. It is assumed that the flow is supersonic along one of the spatial coordinates. Then, the equation (1) is hyperbolic along this coordinate. In particular, the equation (1) is hyperbolic if $u^2 + v^2 > c^2$. Hyperbolicity in the direction of the x direction takes place if $u^2 > c^2$, and hyperbolicity along the y direction takes place if $v^2 > c^2$. For clearance, the case of x-hyperbolicity (the projection of the flow velocity onto the x direction is supersonic) is considered.

The equation (1) is solved by the marching method, which involves step-by-step integration along the x coordinate. A two-dimensional mesh with uniform steps Δx and Δy

in the coordinate directions x and y is constructed. Let's assume that the mesh functions take constant values inside the cells. For the cell interface with number $i + 1/2$, at each step along the x coordinate, the Riemann problem for the equation (1) is solved with the following initial data: $\boldsymbol{U}_i^k = \text{const}$ if $y \leqslant y_{i+1/2}$ and $\boldsymbol{U}_{i+1}^k = \text{const}$ if $y > y_{i+1/2}$. The solution of this problem is denoted by $\boldsymbol{U}_{i+1/2}$. In the same way, the solution vector $\boldsymbol{U}_{i-1/2}$ is found for the interface of the cell with the number $i - 1/2$. The finite volume Godunov scheme for the equations of stationary gas dynamics written in the form (1) has the form

$$\frac{\boldsymbol{F}_i^{k+1} - \boldsymbol{F}_i^k}{\Delta x} + \frac{\boldsymbol{G}_{i+1/2} - \boldsymbol{G}_{i-1/2}}{\Delta y} = 0, \tag{2}$$

where $\boldsymbol{G}_{i\pm1/2} = \boldsymbol{G}(\boldsymbol{U}_{i\pm1/2})$. The superscript $k = 0, 1, \ldots$ denotes the values of the mesh function at step k in x direction. For simplicity, the equation (2) uses the explicit Euler scheme to discretize the derivative with respect to the marching coordinate.

The flow calculation procedure includes the reconstruction of the values of the flow quantities on the faces of the control volumes from the average values over the control volumes and the solution of the Riemann problem. The reconstruction procedure is applied to primitive variables.

The fluxes through the faces of the control volume are found from the relation

$$\boldsymbol{F}_{m+1/2} = \frac{1}{2}\left(\boldsymbol{G}_m^k + \boldsymbol{G}_{m+1}^k\right) + \frac{1}{2}|A|_{m+1/2}^k \left(\boldsymbol{F}_m^k - \boldsymbol{F}_{m+1}^k\right),$$

where $A = (\partial \boldsymbol{G}/\partial \boldsymbol{U})(\partial \boldsymbol{F}/\partial \boldsymbol{U})^{-1}$.

A spectral method of the stability of the linearized equation (1) leads to the following condition

$$C = \max|\lambda_\pm|\frac{\Delta x}{\Delta y} \leqslant 1,$$

where

$$\lambda_\pm = \frac{uv \pm c(u^2 + v^2 - c^2)^{1/2}}{u^2 - c^2}.$$

The speed of sound is found from the relation

$$c = \left[(\gamma - 1)h - \frac{1}{2}(\gamma - 1)(u^2 + v^2)\right]^{1/2},$$

where h is total enthalpy.

The implementation of the scheme (2) is reduced to solving a system of non-linear equations. Godunov's method is based on the exact solution of the Riemann problem. The exact solution of the general Riemann problem consists of two waves (a shock wave or a simple rarefaction wave) with a tangential discontinuity between them, which are separated from each other by regions of uniform flow. The solution is a stationary flow pattern that arises in the region $x > 0$ during the interaction of two uniform semi-unlimited supersonic gas flows meeting on a straight line $y = 0$.

The difference scheme (2) has the first order of accuracy. Higher-order schemes are constructed using the same methods as for the case of unsteady equations. For integration over the marching direction, the three-step Runge–Kutta method is used.

3.2 Particles

The motion of a spherical particle with a diameter of d_p, which is affected only by the drag force, is described by the equation

$$m_p \frac{d\boldsymbol{v}_p}{dt} = \frac{1}{2} C_D \rho \left|\boldsymbol{v} - \boldsymbol{v}_p\right| \left(\boldsymbol{v} - \boldsymbol{v}_p\right) S_p, \tag{3}$$

where m_p is particle mass, S_p is particle midsection area (for a sphere, $m_p = \pi \rho_p d_p^3/6$ and $S_p = \pi d_p^2/4$). The drag coefficient is represented as

$$C_D = \frac{24}{\mathrm{Re}_p} f_D(\mathrm{Re}_p, \mathrm{M}_p, \mathrm{Kn}_p).$$

The function f_D takes into account the correction for the inertia of the particle, the compressibility and rarefaction of the carrier flow. The Reynolds, Mach and Knudsen numbers are calculated from the relative velocity of the gas and particle

$$\mathrm{Re}_p = \frac{\rho \left|\boldsymbol{v} - \boldsymbol{v}_p\right| d_p}{\mu}, \quad \mathrm{M}_p = \frac{\left|\boldsymbol{v} - \boldsymbol{v}_p\right|}{c}, \quad \mathrm{Kn}_p = \frac{l}{d_p},$$

where μ is dynamic viscosity, c is speed of sound, l is mean free path of molecules.

Taking into account the representation of the drag force, the particle motion equation (3) is written as

$$m_p \frac{d\boldsymbol{v}_p}{dt} = 3\pi d_p \mu f_D \left(\boldsymbol{v} - \boldsymbol{v}_p\right). \tag{4}$$

A kinematic relation is added to the equation (4), which makes it possible to calculate the radius vector of the particle's center of mass

$$\frac{d\boldsymbol{r}_p}{dt} = \boldsymbol{v}_p. \tag{5}$$

The temperature equation describing the convective heat transfer between a spherical particle and a gas is written as

$$c_p^m m_p \frac{dT_p}{dt} = \frac{\mathrm{Nu}_p \lambda}{2r_p} S_p \left(T - T_p\right), \tag{6}$$

where c_p^m is specific heat capacity of particle material, S_p is particle surface area, T and T_p are temperature of gas and temperature of particle, respectively. To calculate the Nusselt number, the following formula is used

$$\mathrm{Nu}_p = \mathrm{Nu}_{p0} f_(\mathrm{Re}_p, \mathrm{M}_p, \mathrm{Kn}_p, \mathrm{Pr}),$$

where the value $\mathrm{Nu}_{p0} = 2$ corresponds to the Stokes flow around a rigid sphere. The function f_T takes into account the correction for particle inertia, gas compressibility and rarefaction. The temperature of a particle affects its motion through a correction to the drag coefficient. In many flow regimes, this correction is small and is not taken into account.

At low Reynolds numbers, the drag of a spherical particle is determined in the Stokes approximation. With an increase in the flow velocity, effects associated with the influence

of viscosity and the deviation of drag from the Stokes law begin to appear. In addition to viscosity, there are other factors that affect the drag coefficient. These factors include the influence of the effect of the compressibility, which manifests itself at a significant value of the Mach number, and the effect of the rarefaction of gas, which is estimated by the value of the Knudsen number.

The flow around a particle is characterized by the Knudsen number $\mathrm{Kn}_p \sim \gamma^{1/2}\mathrm{M}_p/\mathrm{Re}_p$. If $\mathrm{M}_p/\mathrm{Re}_p \ll 1$, the continuous flow regime is realized. If $\mathrm{M}_p/\mathrm{Re}_p \gg 1$, free molecular flow around the particle is realized. A transitional flow regime takes place between continuous and free molecular regimes.

The most common of the numerous dependencies for the drag coefficient available in the literature are the Henderson relationships [40]. The experimental data used in [40] have an accuracy of $\pm 2\%$. The relationships consist of a relation describing subsonic flow regimes, a relationship describing supersonic flow regimes at $\mathrm{M} > 1.75$, and a linear interpolation relationship for transition flow regimes. The Henderson formula is applicable to Mach numbers $\mathrm{M} \leqslant 6$, any Knudsen numbers, and subcritical Reynolds numbers $0 < \mathrm{Re} < 10^5$, leading to the Stokes and Oseen solutions. Despite the complex nature and various regimes of flow around a sphere, the Henderson relations make it possible to calculate the drag coefficient with a high accuracy (about 10%), which is acceptable for practical calculations.

In addition to determining the drag force, there is a need to describe the heat flux between a particle and surrounding. For small particles, Newton's law of cooling is applied. To determine the heat transfer coefficient, the Nusselt number is calculated taking into account the influence of the effects of viscosity, compressibility and rarefaction.

Integration of the equations (4)–(6) requires setting initial conditions at time $t = 0$. In an undisturbed flow, a particle moves along streamlines with velocity and temperature equal to flow.

4 Computational domain and boundary conditions

The computational domain consists of the supersonic part of the nozzle and the space into which the jet flows. The nozzle has a cylindrical inlet section. The geometric configuration of the nozzle is schematically shown in Figure 2 (the parameters with the dimension of length are normalized to the radius of the throat of the nozzle r_c). The radii of the inlet and outlet sections of the nozzle are assumed to be equal to $r_i = 3$ and $r_o = 5$, the lengths of the inlet cylindrical section (the length of the combustion chamber) and the expanding socket of the nozzle is $l_i = 5$ and $l_o = 10$, the radius rounding at the inlet to the subsonic part of the nozzle and rounding radius at the critical point are $r_1 = 5$ and $r_2 = 7.5$.

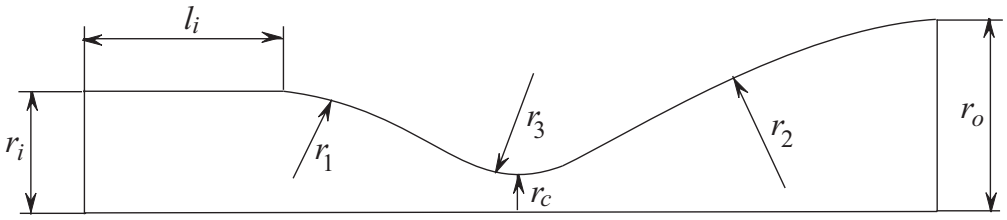

Figure 2. Geometry of nozzle

Calculations are carried out at various nozzle pressure ratios. The parameter $n = p_a/p_\infty$ is defined as the ratio of the static pressure at the nozzle outlet to the atmospheric pressure.

It varies due to variation in the atmospheric pressure, which corresponds to different flight altitudes. The air quantities at a given altitude correspond to the standard atmosphere model.

In the case when a rarefaction flow of a plane supersonic flow occurs, the Prandtl–Meyer flow is realized with a fan of the characteristics of the first family and the constancy of the flow quantities on them. There is a smooth expansion of the flow, in which there are no shock-wave structures. The Prandtl–Meyer flow is realized as long as the flow quantities are not affected by the characteristic reflected from the symmetry plane. In the case when the expansion flow is realized in an axisymmetric uniform flow, the flow pattern differs from the Prandtl–Meyer flow. In the region where the expansion of the nozzle flow begins, the axisymmetric flow causes a noticeable deviation from the Prandtl–Meyer expansion. The jet boundary is bent, and conditions are created for the formation of a shock wave.

5 Numerical method

The flow of an ideal gas is described by the Euler equations written in a conservative form. The boundary conditions for governing equations are the no-penetration conditions on the nozzle wall, the condition for the formation of a flow with a given pressure on the free streamline, and the conditions on the centerline.

For calculations, the marching method is used, which is based on a finite volume approach to the discretization of the governing equations with the construction of the faces of the control volume along the streamlines. The local problem of constructing a face and determining the flows on it is solved on the basis of the Riemann problem. Its implementation for calculating supersonic stationary ideal gas flows are discussed in [18, 19]. A non-uniform initial mesh with thickening near the nozzle outlet is set. Local adaptation of the mesh is carried out in the region of jet formation [41].

There are two approaches to constructing distributions of flow quantities in the inlet section of the computational domain. In one of the approaches, the flow in the subsonic part of the nozzle and some part of the transonic region is preliminarily constructed on the basis of the Godunov method for calculation. The final section of this region, in which the supersonic flow is realized, is taken as the initial section of the combustion chamber. This approach is workable, but demanding on computing resources. To conduct parametric studies, a simplified approach is applied, in which the throat of the nozzle is taken as the initial section, in which the condition of a parallel uniform flow with a small supersonic speed is set. It is usually sufficient to take the Mach number in the inlet section equal to 1.05.

6 Prandtl–Meyer flow

To clarify the details of formation of a reversed flow near the edge of the nozzle, a study of the flow around the corner element at the edge of the nozzle is carried out. The expansion of the flow in supersonic flow around an external corner occurs with the formation of a centered rarefaction wave defined by a fan of straight Mach lines emanating from the corner (Figure 3). Three flow regions are formed: an uniform inlet flow with Mach number M_1 (region 1), a plane-parallel supersonic flow with Mach number $M_2 > M_1$ along the wall, located at an angle δ to the inlet flow (region 3), and the region of a centered rarefaction wave, in which the flow turns and isentropically expands (region 2). The flow expansion region is located

between two Mach lines forming an angle $\mu = \mu_1 - \mu_2$. The slope of the first characteristic (on the side of the inlet flow) μ_1 corresponds to the Mach number of the inlet flow M_1, and the slope of the last characteristic μ_2 corresponds to the Mach number M_2. The slope of the characteristic i is related to the Mach number by the relation $\mu_i = \arcsin(1/M_i)$.

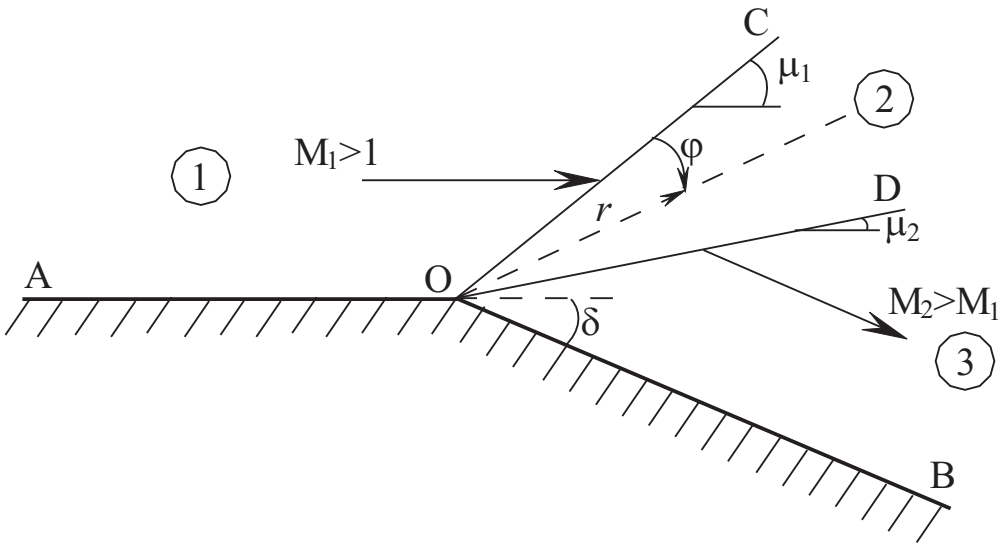

Figure 3. Supersonic flow around expansion corner

Calculations are carried out for aluminum oxide particles with density $\rho_p = 3600$ kg/m^3 and specific heat capacity $c_p^m = 880$ J/(kg·K). In an undisturbed flow, the Mach number, density and temperature of the gas ($\rho_0 = 0.221$ kg/m^3, $T_0 = 1570$ K) are specified. Working environment is air ($\gamma = 1.4$). The viscosity and thermal conductivity of the gas are neglected, except for the interaction of gas with particles. Thermophysical parameters of air are reference, taking into account their dependence on temperature. The dependence of viscosity on temperature is taken into account using the dependence $\mu/\mu_* = (T/T_*)^n$, where $n = 0.5$, $\mu_* = 1.71 \times 10^{-5}$ Pa·s at a reference temperature $T_* = 293$ K. It is assumed that the relative velocity of the gas and the particle is zero until the particle reaches the first characteristic (the two-phase flow is in equilibrium). The slope of the first characteristic is determined by the Mach number of the undisturbed flow.

The motion of a particle is determined by a dimensionless parameter that depends on the initial radial coordinate of the particle r_0, the thermophysical properties of the gas, determined by the adiabatic exponent γ, and the conditions in the undisturbed flow [20]

$$R_0 = \frac{\gamma + 1}{\gamma - 1} \frac{r_0}{\tau_p \mathrm{M}_0 c}.$$

The theoretical maximum flow expansion speed is found from the relationship

$$c^2 = 2c_p T_0 \left(1 + \frac{\gamma - 1}{2} \mathrm{M}_0^2\right).$$

Index 0 corresponds to the parameters of the gas and particles before they enter the disturbed flow region. The particle relaxation time is found as $\tau_p = \rho_p d_p^2/(18\mu)$.

It should be noted that the conditions in the undisturbed flow have a relatively weak effect on the parameter R_0. The parameter R_0 depends mainly on the particle size d_p and

the initial radial coordinate of the particle r_0. For particles of micron diameter located at a distance of several centimeters from the corner point, $R_0 > 10$.

In the calculations, the value of the angle of deviation of the flow (from 0 to 60 degrees), the diameter of the particles, and the coordinates of the point where the particles enter the flow vary. The deflection angle of the flow is related to the Mach number of the undisturbed flow using the Prandtl–Meyer relations. The parameter R_0 varies from 0.01 to 50 by changing the particle diameter and the initial radial coordinate of the particle. The particle diameter is assumed to be 1 and 4 m.

The trajectories of Stokes particles are shown in Figure 4 at $M_0 = 1.4$. When moving around the expansion corner, the particles deviate from the streamlines of the carrier flow, and this deviation increases with an increase in the size of the particles and their initial radial coordinate. In particular, for $R_0 > 50$ the particles follow the streamlines of the carrier flow (line 6), and the relative velocity of the gas and the particle is equal to zero. Reducing the parameter to $R_0 < 1$ leads to the deviation of the particles from the streamlines and a significant velocity lag (lines 1–3).

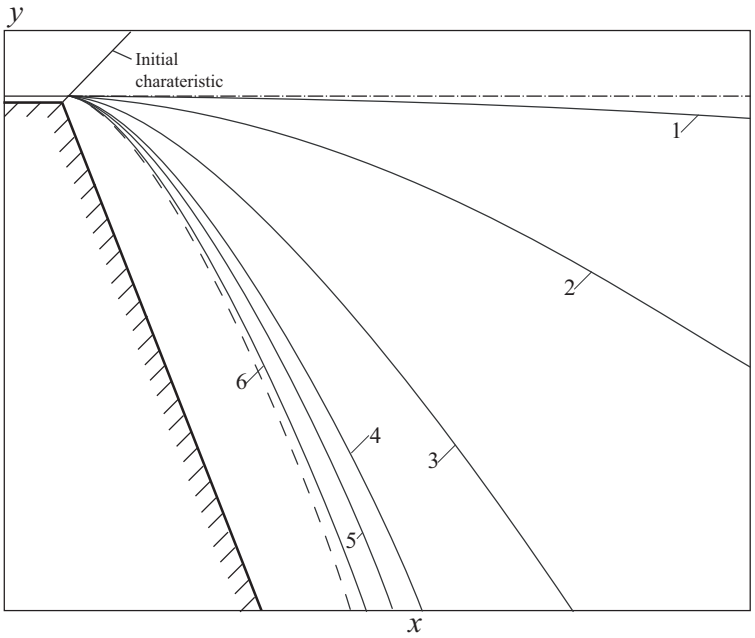

Figure 4. Particle trajectories in the flow around the expansion corner at $R_0 = 0.01$ (1); 0.1 (2); 1 (3); 5 (4); 10 (5); 50 (6). The dashed line corresponds to the streamline, and the dotted line corresponds to the zero flow deflection angle

The flow in the radial and tangential directions is characterized by the relative velocities $v_{sr}/v_r = (v_r - v_{pr})/v_r$ and $v_{s\varphi}/v = (v_\varphi - v_{p\varphi})/v_\varphi$. Figure 5 shows the change in the relative velocity of gas and particles depending on the angle of flow deflection at a fixed Mach number ($M_0 = 1.4$). The non-equilibrium flow velocity in the tangential direction significantly exceeds the flow velocity in the radial direction. At $R_0 = 0.01$ (line 1) there is a significant velocity lag in the tangential direction, and the particles deviate relatively weakly from the direction of the undisturbed flow. The maximum relative velocity of the gas and particles in the radial direction reaches 0.162 at $\theta = 25°$. Near this point, the relative Mach number is about 0.002, and the relative Reynolds number is 8 for particles with a diameter of 4 μm.

At $R_0 = 10$ (line 5), the maximum relative velocity in the radial direction is less than 1%, and the relative Mach number and relative Reynolds number are 0.152 and 2 for particles with a diameter of 4 μm.

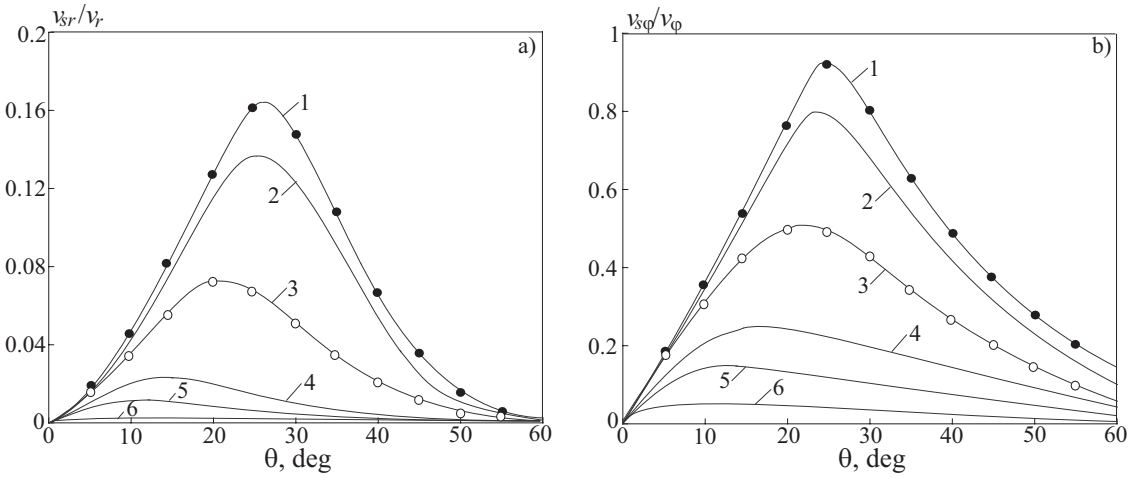

Figure 5. Distributions of relative radial (a) and tangential (b) velocities of gas and particles at $R_0 = 0.01$ (1, •); 0.1 (2); 1 (3, ∘); 5 (4); 10(5); 50(6). The symbols • and ∘ correspond to data from [20] for the conditions described by lines 1 and 3

A change in the exponent as a function of viscosity from temperature from 0.5 to 1 leads to a slight perturbation of the particle trajectories. In this case, the change in the velocity of the particle relative to the gas in the tangential direction changes by several percent, while the sliding velocity in the radial direction remains unchanged.

A change in the thermophysical parameters of the gas, characterized by the adiabatic exponent, has a more significant effect on the particle trajectory and velocity lag. As the adiabatic index decreases from 1.4 to 1.2, the relative velocity of the particle in the tangential direction increases, which is expressed in an increase in the deviation of the particle trajectory from the streamline. A decrease in the adiabatic index has a relatively weak effect on the change in the relative velocity of the particle in the radial direction.

During the Prandtl–Meyer flow, the Knudsen number for micron-sized particles varies over a wide range, which should be taken into account in calculating the correction for the rarefaction to the drag coefficient. As the particle diameter decreases, the role of the correction to the Stokes drag law increases.

Figure 6 shows the influence of the correction to the drag law at $M_0 = 3$ for particles with a diameter of 1 and 4 μm. In contrast to the motion of Stokes particles, when the correction to the drag coefficient is taken into account, particles with a diameter of 1 μm at $R_0 = 50$ (line 3) do not follow the streamlines, and at $R_0 = 0.1$ (line 1) there is a significant deviation of particle trajectories from undisturbed flow direction. In particular, at $R_0 = 0.1$ for particles with a diameter of 4 μm, whose drag deviates from the Stokes law, the maximum relative Mach number and Reynolds number are 0.922 and 6.68, while for Stokes particles these values decrease to 0.852 and 6.49, respectively. A significant effect of the correction to the Stokes drag law on the relative velocity of particles and gas is also observed (Figure 7).

The effect of particles on the ratio of pressures and temperatures in a rarefaction wave is shown in Figure 8. The angle varies from 0 to 60 degrees. The mass concentration of the dispersed phase is $\kappa_p = 0.25$. The presence of particles of the dispersed phase leads to a slower decrease in pressure and temperature (dashed lines) compared to the flow of pure gas

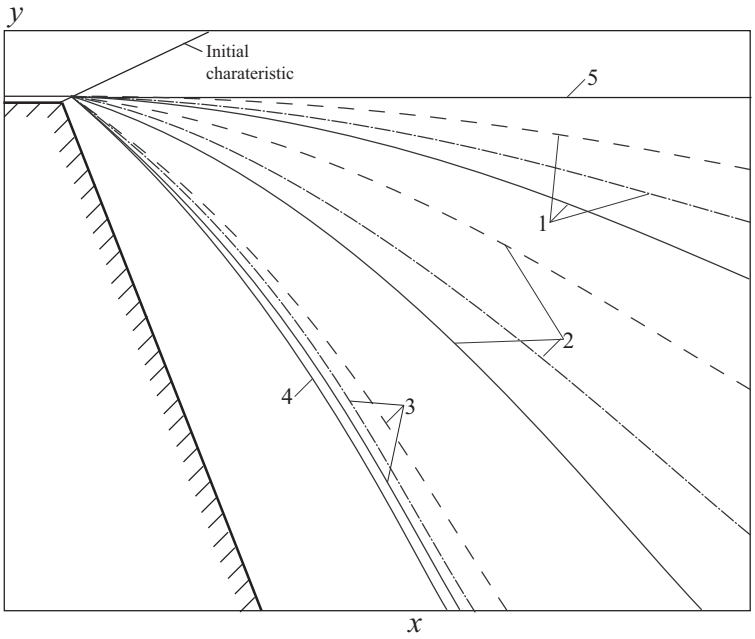

Figure 6. Particle trajectories in the flow around the expansion corner at $R_0 = 0.1$ (1); 12); 50(3). The solid lines correspond to the trajectories of Stokes particles, the dotted and dash-dotted lines correspond to the trajectories of particles with a diameter of 1 and 4 μm, calculated taking into account the correction to the drag law. Lines 4 and 5 correspond to the streamline of the carrier flow and zero deflection angle of the stream

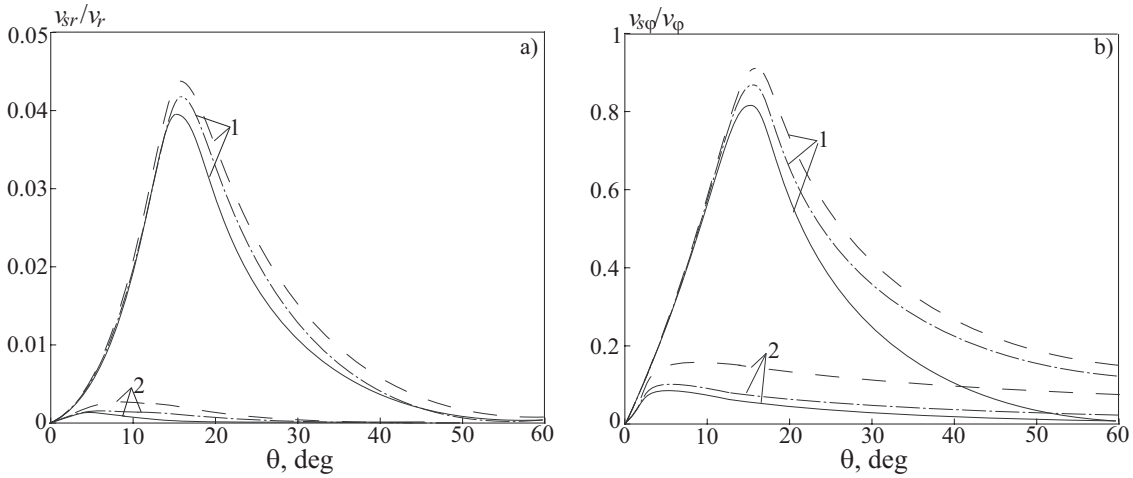

Figure 7. Distributions of relative radial (a) and tangential (b) velocity of gas and particles at $R_0 = 0.1$ (1); 50(2). The solid lines correspond to Stokes particles, the dotted and dash-dotted lines correspond to the distributions of particles with a diameter of 1 and 4 μm, calculated taking into account the correction to the drag law

(solid lines).

When a two-phase flow interacts with the expansion corner, a particle-free flow zone is formed. A similar flow structure is observed when the two-phase flow expands in the nozzle. The influence of particles leads to an increase in the deflection angle of the flow compared to pure gas (Table 1). When the Mach number of the undisturbed flow changes in the range

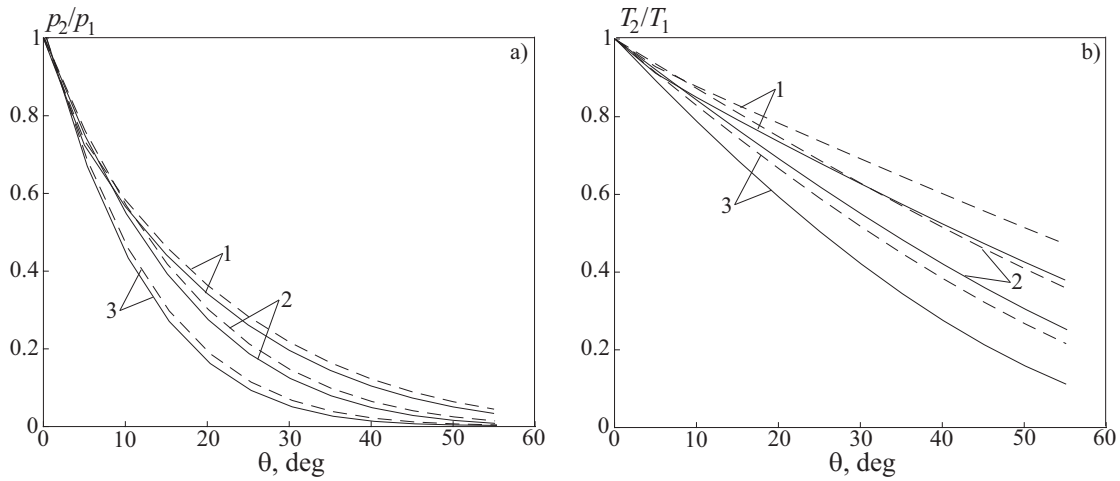

Figure 8. Influence of particles on the ratio of pressures (a) and temperatures (b) in a rarefaction wave at $M_1 = 1$ (1); 2(2); 3(3). The solid lines correspond to the flow of pure gas, and the dotted lines correspond to the gas-particle flow

from 1 to 3, the maximum deviation angle of the flow increases by approximately 15 degrees as compared to the pure gas flow.

Table 1. Influence of particles on the maximum deflection angle of the flow

Parameter	Pure gas			Gas with particles		
M_1	1	2	3	1	2	3
θ_{max}, deg	130.45	104.69	80.70	145.55	120.65	94.88

It follows from the Prandtl–Meyer solution that for an inviscid flow there is a limiting deflection angle at which the internal energy of the gas is converted into the kinetic energy of motion, as a result of which the flow temperature vanishes and the Mach number increases to infinity. Viscous effects can significantly change the flow and, in particular, contribute to the vortical flow at large angles and the formation of a reversed flow. The role of viscous forces increases as the flow expands and begins to prevail over the rarefied regime. In contrast to the Prandtl–Meyer solution for an inviscid gas, the effect of viscosity leads to a decrease in the Mach number and an increase in temperature.

The wave pattern in a viscous flow past an external corner is complicated by the interaction of rarefaction waves with the boundary layer. In a rarefaction wave passing through the boundary layer in the zone of its turn, the flow is not isentropic. The consequence of this interaction is the misalignment of the characteristics of the Prandtl–Meyer wave, a change in the angle of their inclination in the external flow, as well as the formation of a shock wave and a tangential discontinuity located below the shock. The lines of constant pressure in the region of flow expansion are not straight, and the angle of flow direction is less than the total angle of the Prandtl–Meyer flow required to achieve the same pressure. Comparison of the results with experimental data shows that the effect of reduced pressure upstream from the expansion corner affects the distance on the order of the boundary layer thickness. The pressure on the inclined wall decreases to a value corresponding to an inviscid flow.

7 Nozzle flow

The nozzle has a critical section diameter of 250 mm. The diameter of the outlet section is 5 times larger. The pressure and temperature in the combustion chamber are 80 atm and 3851 K. A gas with a ratio of specific heat capacities of 1.2 and a gas constant of 336.9 J/kg is used. The gas expands to the space with a pressure of 1600 Pa and a density of 0.0179 kg/m^3, which corresponds to altitude of 30,000 m.

The distribution of flow quantities along the nozzle centerline is shown in Figure 9. The obtained distributions of the Mach number and temperature are in good agreement with the data obtained from the theory of isentropic flow of an inviscid compressible gas in a Laval nozzle.

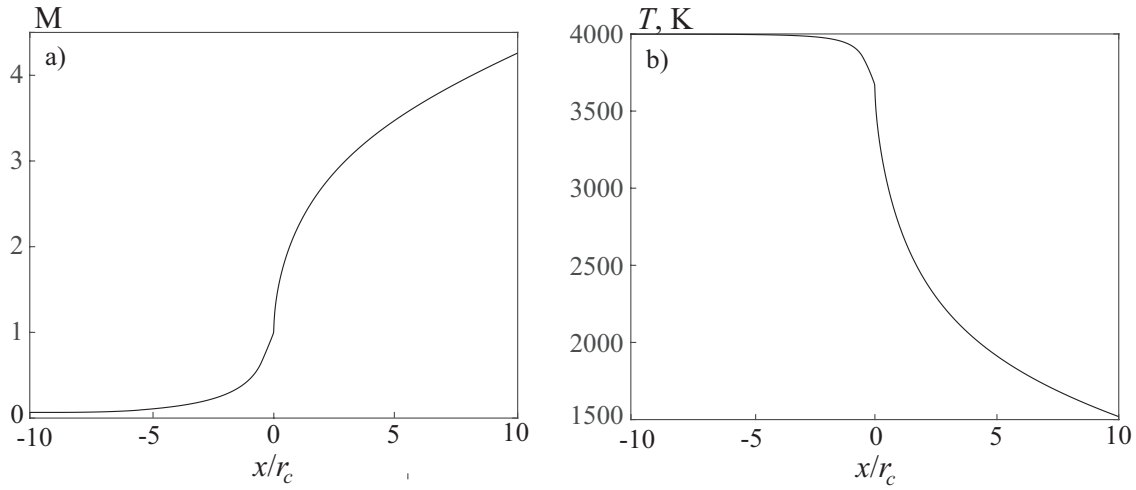

Figure 9. Distributions of Mach number (a) and temperature (b) along the nozzle centerline

The results of flow calculations in the nozzle and jet, processed as Mach number level lines, are shown in Figure 10 (transonic, supersonic part of the nozzle and jet). The calculations use two methods of setting the boundary conditions at the jet boundary. In one approach, a static pressure is specified at the jet boundary, while in the other, the boundary conditions are formulated according to Newton method. The results of calculations obtained with different methods of setting the boundary conditions at the jet boundary are in good agreement with each other. Although Newton's method is less accurate, its advantage is that there are no restrictions on the co-flow velocity. In particular, at low atmospheric pressures (of the order of 1600 Pa), a zone with subsonic velocities appears in the co-current near the jet boundary, which makes it impossible to use the marching method with strict boundary conditions.

Particles of different sizes are introduced into the flow at the throat of the nozzle or in a cross section near the nozzle exit. Figure 11 shows the distributions of velocity and particles of various sizes along the nozzle centerline.

The results of numerical simulation of two-phase flows, processed as dependencies of the Mach number and pressure on the axial coordinate, are shown in Figure 12 for $n = 0.6$. The mass concentration of the dispersed phase is $\kappa_p = 0.2$. The particle density is $\rho_p = 2800$ kg/m^3, their diameter is $d_p = 5$ μm. The solid line corresponds to the flow of pure gas, and the symbols $\square$ correspond to particles. The results presented show that the difference scheme smears the discontinuity into 1–2 computational cells, while the monotonic nature

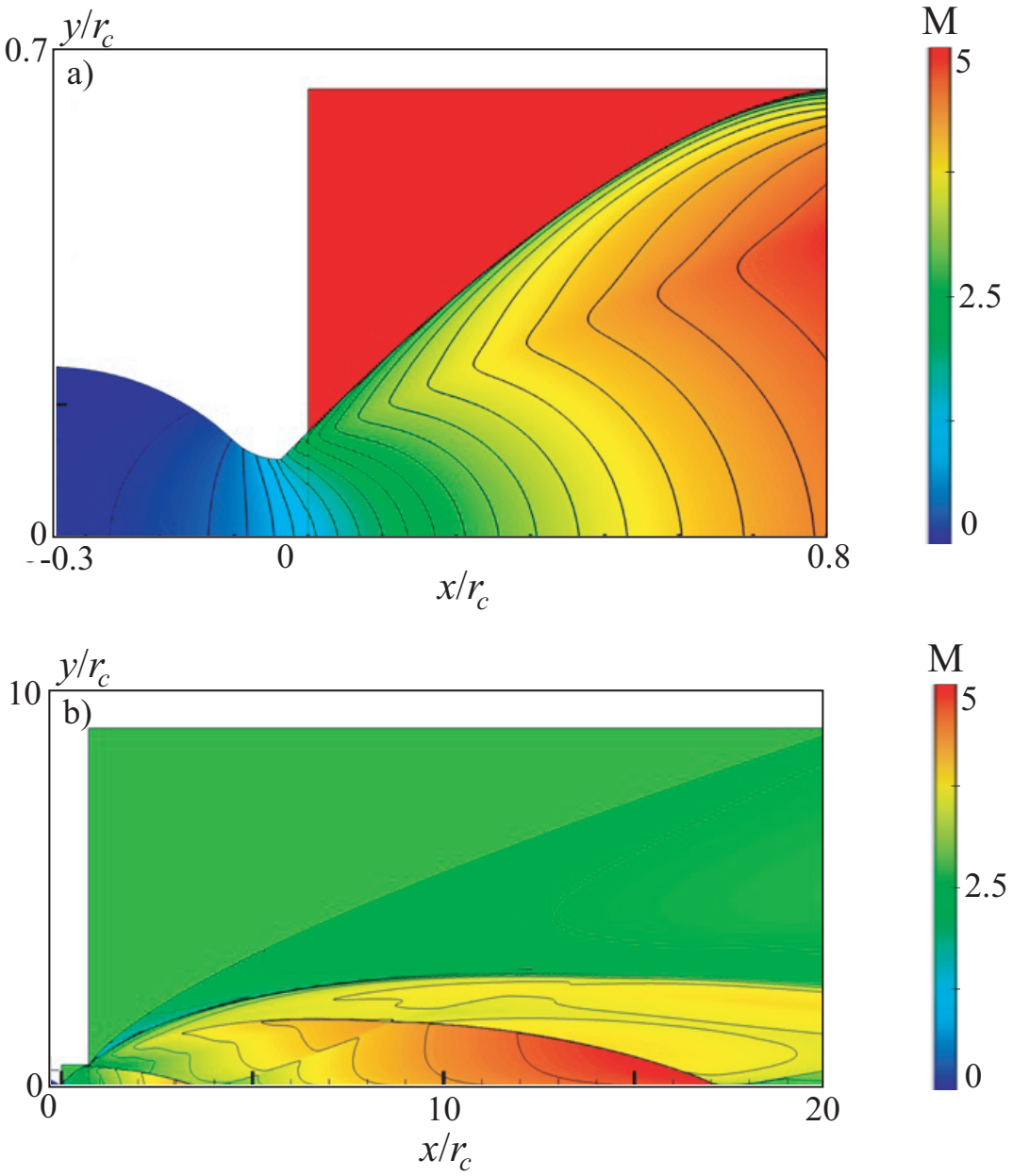

Figure 10. Contours of Mach number in nozzle (a) and jet (b)

of the solution is preserved (there are no computational oscillations).

Another calculated flow regime corresponds to the case when the flow is continuously expands along the nozzle centerline. The results obtained are shown in Figure 13 for a pressure drop of $n = 0.2$. The mass concentration of the dispersed phase is $\kappa_p = 0.2$.

When a mixture of gas with particles moves in a nozzle, two-dimensional effects play a significant role both because of the uneven distribution of particles in different sections of the nozzle and because of the possible deposition of particles on the walls in the subsonic and supersonic parts of the nozzle. As a result, the particle trajectories differ from the gas streamlines, and the particle velocity and their temperature in the trans- and supersonic parts depend on the flow quantities in the subsonic region.

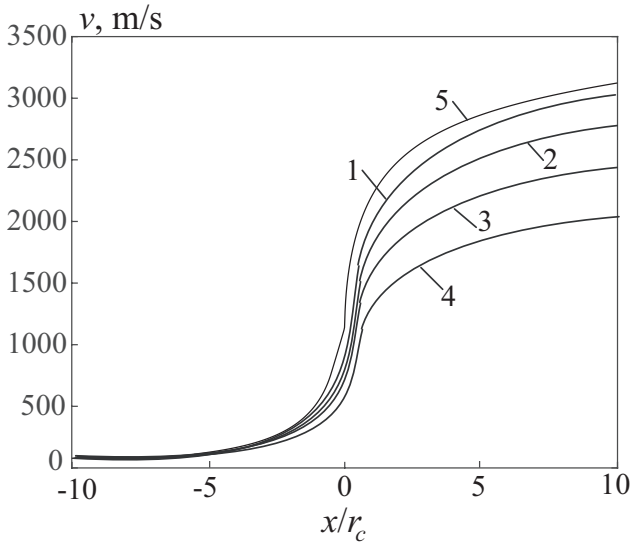

Figure 11. Distributions of gas velocity (line 5) and particle velocity with a diameter of 5 μm (line 1), 25 μm (line 2), 50 μm (line 3), 100 μm (line 4) along the nozzle centerline

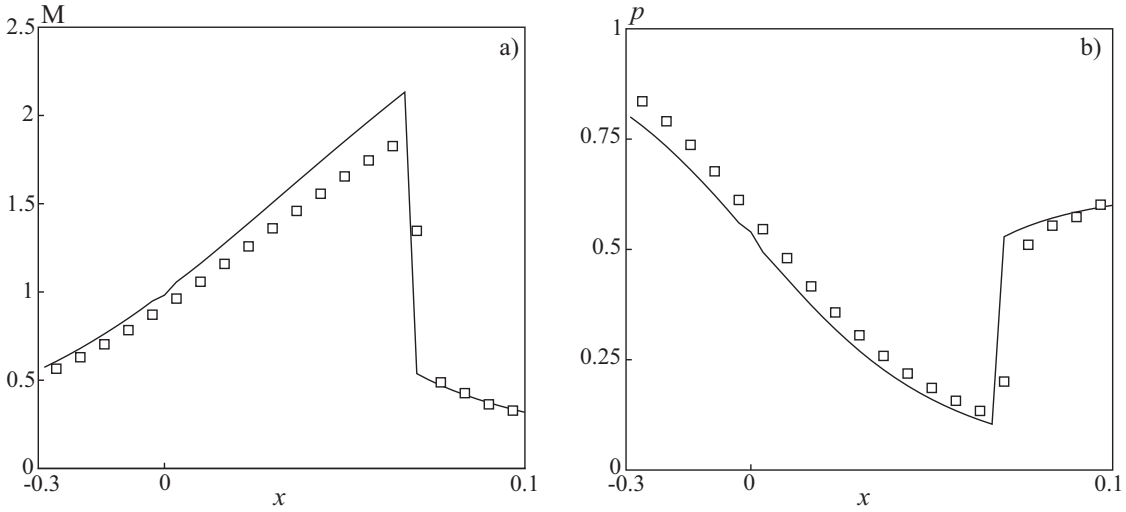

Figure 12. Distributions of Mach number (a) and pressure (b) along the nozzle centerline at $\kappa_p = 0.2$ in the case of underexpanded flow

8 Jet flow

The marching calculations of jets start from the nozzle outlet, where two flows are specified, an internal flow of combustion products and an external air flow (if any).

When the ratio of pressures is less than critical, the gas flow expires at subsonic speed, and further expansion of the flow is impossible. When the pressure ratio exceeds the critical value, the flow becomes supersonic, and with increasing distance from the nozzle, the Mach number increases. The expansion of the gas occurs outside the nozzle and in the initial section propagates along a rarefaction wave centered at the nozzle outlet. The flow in this region is overexpanded with respect to the external pressure and is limited by oblique shock waves. The jet flow consists of compression and rarefaction regions. As the pressure ratio

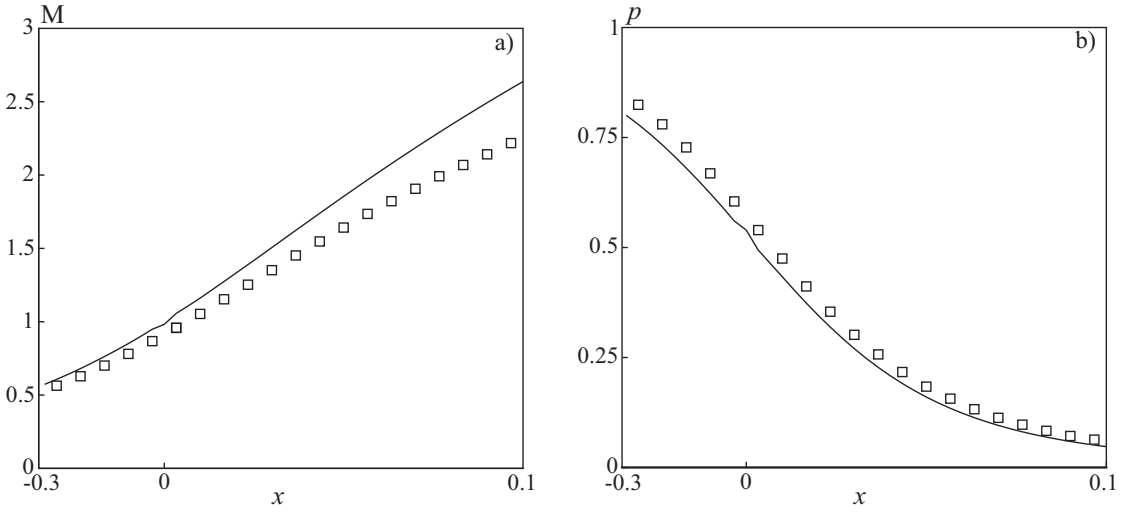

Figure 13. Distributions of Mach number (a) and pressure (b) along the nozzle centerline at $\kappa_p = 0.2$ in the case of overexpanded flow

p_a/p_∞ increases, the characteristic dimensions of an axisymmetric jet of an ideal gas increase proportionally to $(p_a/p_\infty)^{1/2}$. A characteristic feature of the flow in a strongly underexpanded ideal gas jet is the presence in its initial section of a region that does not depend on external conditions and corresponds to the flow expansion into vacuum. The flow asymptotically tends to flow from a source with a variable critical section radius.

When the gas expands into vacuum, the pressure does not affect the jet, and the jet expands freely. In the limiting case, when the gas flows into vacuum, shock waves do not arise in the jet. At the edge of the nozzle, the flow turns to the maximum possible deflection angle, and at distances exceeding the size of the outlet section of the nozzle, the jet acquires the character of a flow with an intensity distributed over the polar angle. In this case, the gas velocity reaches the limiting value $v_{\max} = (2H_0)^{1/2}$, where H_0 is the total enthalpy, and the streamlines approach straight lines.

The Mach number distributions at different altitudes are shown in Figures from 14 to 16. The Mach number in the initial section of the computational domain (it is located close to the critical section of the nozzle) is assumed to be 1.05, and the pressure and density are fixed at 4 MPa and 3.6 kg/m^3. The ratio of specific heat capacities is 1.25. With an increase in altitude (a decrease in atmospheric pressure), the flow reverses and a reversed flow is formed. While the flow structure in the jet near the centerline changes relatively little, the angle of flow reversal near the nozzle outlet depends on the atmospheric pressure.

At the edge of the nozzle, the flow makes a sharp turn, forming a reversed flow. The streamlines in the reversed flow begin to diverge from one point at the edge of the nozzle. Consideration of the streamlines inside the nozzle shows that the entire volume of gas involved in the counterflow comes from a thin near-wall layer. In calculations, this layer is located within one cell of the computational mesh closest to the wall. The gas flow in the counterflow is quite small. In this case, the shape of the edge has a rather weak effect on the flow.

Large particles interact more weakly with the gas phase, which is expressed in their slower cooling when moving in the supersonic part of the nozzle. Lagging behind the gas phase in velocity leads to the fact that the separatrix of this fraction of particles strongly deviates from the contour of the nozzle. Large particles in the outlet section of the nozzle

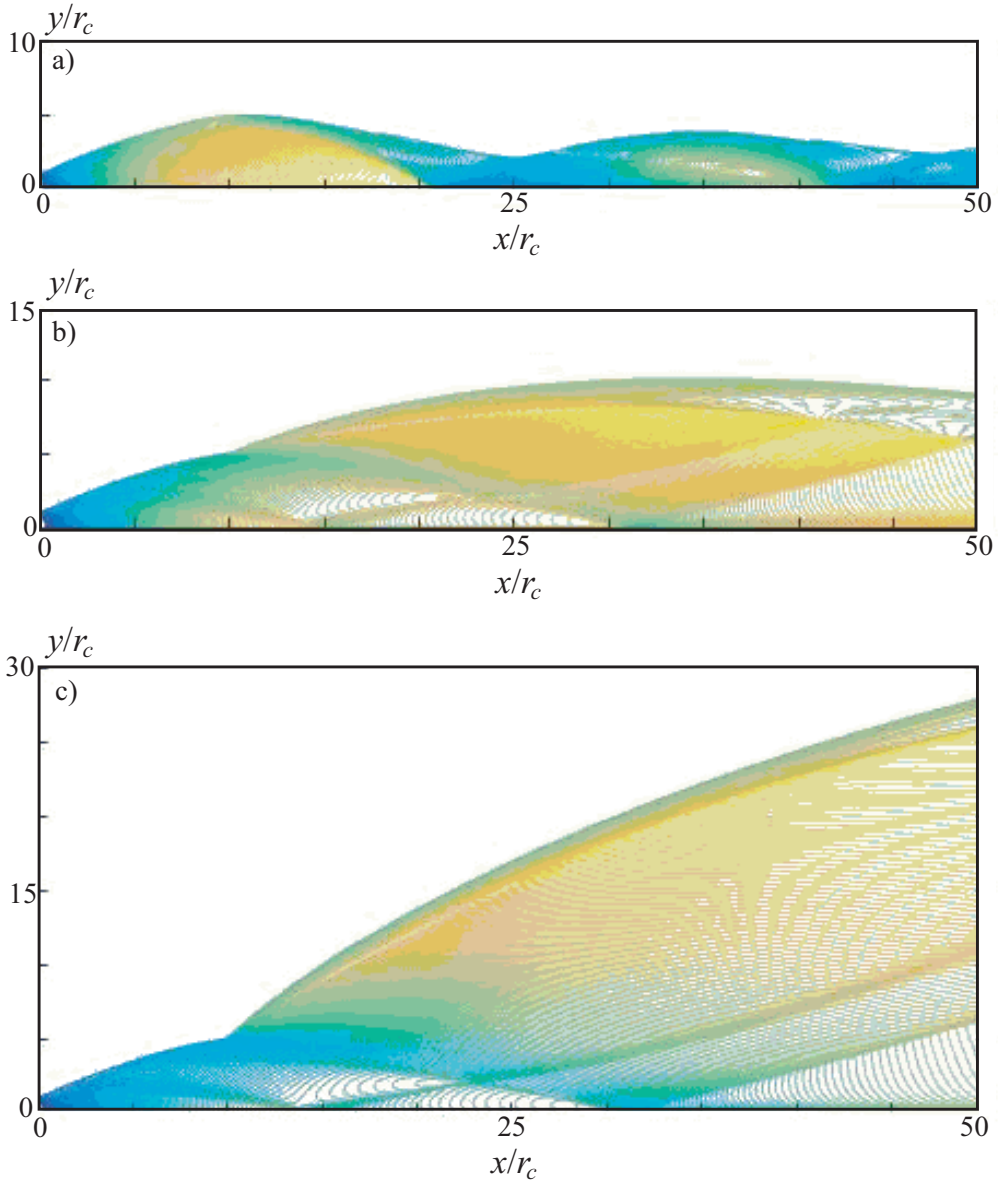

Figure 14. Contours of Mach number on altitude $h = 0$ km (a); 16 km (b); 32 km (c)

are in a liquid state. In the central part of the jet, they remain quite hot, but at the periphery, falling into the cold external flow, they cool down. Intensive cooling of small particles leads to their crystallization, accompanied by a sharp rise in temperature. The influence of the condensed phase on the flow in the jet results in a decrease in the effective value of the adiabatic index and a more intense turn of the streamlines (there is an increase in the characteristic angle of expansion of the jet).

Unlike gas flow, the particles do not make a sharp turn at the edge of the nozzle, and no signs of their movement in the opposite direction are observed. The aerodynamic forces generated by the reversed flow are not sufficient for a sharp inversion of droplets around the edge of the nozzle. The initial position of the droplets (in the throat or near the nozzle exit) does not significantly affect the further movement. Even a small droplet initially placed in the near-wall boundary layer near the nozzle outlet acquires moment components in the flow direction, the value of which turns out to be large, as a result of which the direction of this

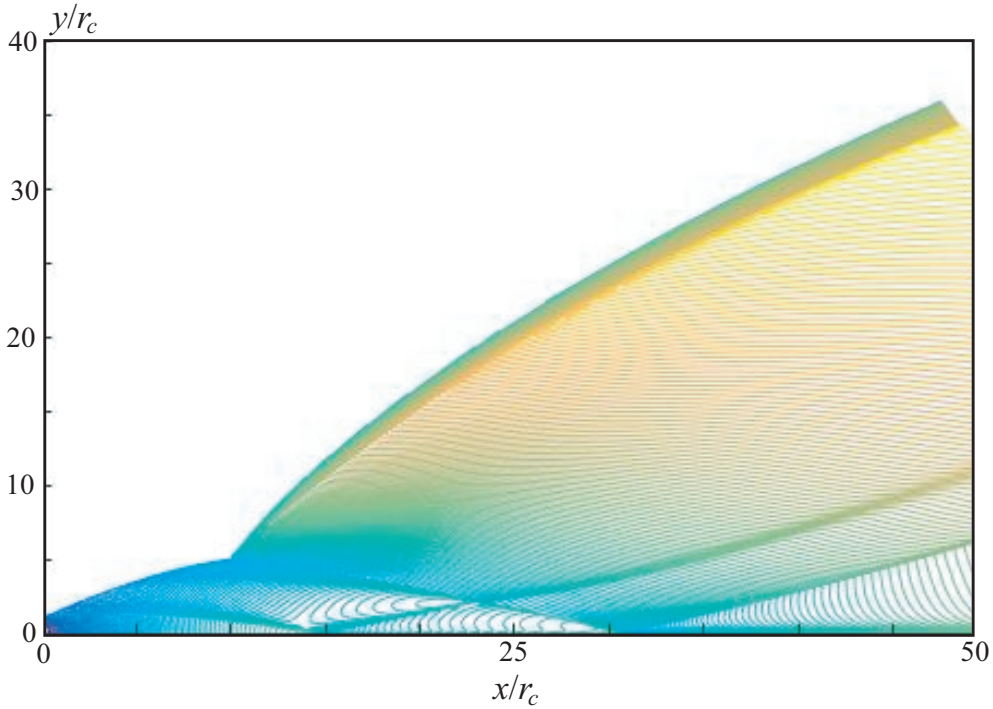

Figure 15. Contours of Mach number on altitude $h = 40$ km

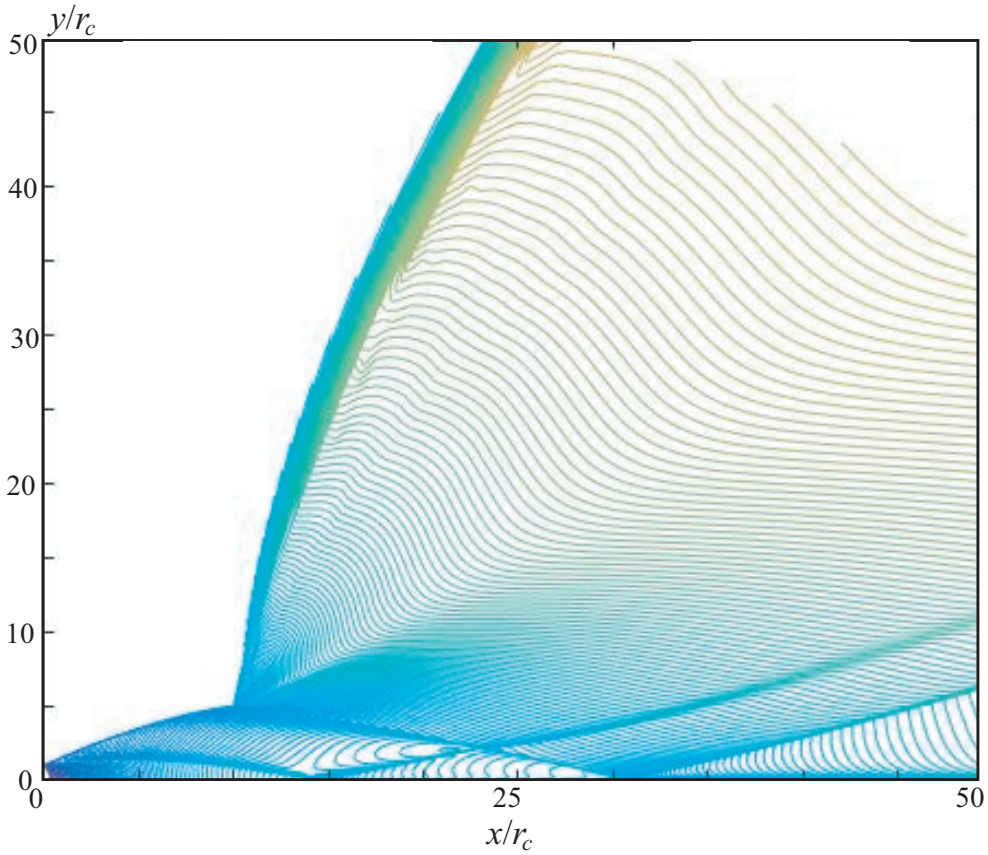

Figure 16. Contours of Mach number on altitude $h = 56$ km

moment vector cannot be changed sharply by the gas in a state of rapid flow around the nozzle edge.

9 Conclusion

Numerical simulation tools have been developed for stationary supersonic flows of an ideal compressible gas in nozzles and jets. The characteristic features of the gas jets expanded into a rarefied atmosphere are considered. The developed tools make it possible to calculate jets expending from nozzles of various shapes into atmosphere with low pressure (on the order of several pascals). The possibilities of applying the developed numerical method to the calculation of flows in nozzles and jets are limited by the condition of the absence of subsonic zones in the flow, when the condition of hyperbolicity of the Euler equations in the marching direction is violated.

A numerical simulation of a gas flow around an external corner containing particles of a spherical shape is carried out. The size of the particles and the coordinates of the entry point of the particle into the flow have a significant effect on the features of their transport in the Prandtl–Meyer flow. When a two-phase flow interacts with an expansion corner, a particle-free flow zone is formed. The presence of particles leads to an increase in the angle of deflection of the flow compared to pure gas, as well as to a slower decrease in pressure and temperature compared to the flow of pure gas.

In the flowfield of a jet expanding into a vacuum, due to gas expansion and a decrease in density, at some distance from the nozzle outlet, the mean free path of molecules become comparable with the characteristic flow dimensions, i.e. there is a violation of the continuity of the flow. The flow passes through all flow regimes from continuous flow in the combustion chamber and nozzle to free molecular flow in the jet at a large distance from the nozzle outlet and is essentially non-equilibrium. At a certain distance from the nozzle outlet, the flow is broken when the mean free path of molecules becomes comparable with the characteristic size of a flow. This circumstance does not allow using continuum methods (Euler or Navier–Stokes equations) to calculate the entire flowfield. In the transitional and free molecular regimes, it is necessary to use the methods of molecular gas dynamics.

Acknowledgments

The research was supported by Russian Science Foundation No. 21-19-00657,
https://rscf.ru/en/project/21-19-00657/

References

[1] V.N. Yarygin, V.G. Prikhodko, I.V. Yarygin, Yu. N. Vyazov, Effect of physical properties of liquid on the outflow of the wall liquid film with the co-current gas flow from the nozzle in-to vacuum, Thermophysics and Aeromechanics 22 (2015) 651–653.

[2] V.B. Betelin, N.N. Smirnov, V.F. Nikitin, V.R.Dushin, A.G.Kushnirenko, V.A. Nerchenko, Evaporation and ignition of droplets in combustion chambers modeling and simulation, Acta Astronautica 70 (2012) 23–35.

[3] N.N. Smirnov, V.B. Betelin, A.G.Kushnirenko, V.F. Nikitin, V.R.Dushin, V.A. Nerchenko, Ignition of fuel sprays by shock wave mathematical modeling and numerical simulation, Acta Astronautica 87 (2013) 14–29.

[4] L.E. Sternin, Fundamentals of gas dynamics of two-phase flows in nozzles. Moscow, Mashinostroenie, 1974.

[5] K.N. Volkov, V.N. Emelaynov, Gas-particle flows. Moscow, Publishing House of Physical and Mathematical Literature, 2008.

[6] R.K. Chaturvedi, P. Gupta, L.P. Singh, Evolution of weak shock wave in two-dimensional steady supersonic flow in dusty gas, Acta Astronautica 160 (2019) 552–557.

[7] I.S. Yakovenko, A.D. Kiverin, Micro-particles spraying via non-stationary flame acceleration process, Acta Astronautica 181 (2021) 620–632.

[8] C. Li, X. Zhu, J. Wei, Powder feeding in a powder engine under different gas-solid ratios, Acta Astronautica 189 (2021) 712–721.

[9] A.V. Rodionov, New space-marching technique for exhaust plume simulation, AIAA Paper 2000-3390 (2000).

[10] S.M. Dash, D.E. Wolf, J.M. Seiner, Analysis of turbulent under-expanded jets. I. Parabolized Navier–Stokes model, SCIPVIS, AIAA Journal 23 (1985) 505–514.

[11] M. Sibulkin, W.H. Gallaher, Far-field approximation for a nozzle exhausting into vacuum, AIAA Journal 1 (1963) 1452–1453.

[12] F.A. Albini, Approximate computation of underexpanded jet structure, AIAA Journal 3 (1965) 1535–1537.

[13] F.P. Boynton, Highly underexpanded jet structure: exact and approximate calculations, AIAA Journal 5 (1967) 1703–1704.

[14] A.P. Makasheva, A.Zh. Naimanova, Numerical calculations of supersonic underexpanded jets in a cocurrent flow using parabolized Navier–Stokes equations, Journal of Applied Mechanics and Technical Physics 49 (2008) 54–63.

[15] S.M. Dash, D.E. Wolf, Shock-capturing parabolized Navier–Stokes model (SCIPVIS) for the analysis of turbulent underexpended jets, AIAA Paper 83-704 (1983).

[16] A.V. Safronov, Method for calculating the jets of combustion products at the start, Physical and Chemical Kinetics in Gas Dynamics 4 (2006) 1–19.

[17] G. Dettleff, R.D. Doetcher, C. Dankert, G. Koppenwallner, H. Legge, Attitude control thruster plume flow modeling and experiments, Journal of Spacecraft Rockets 23 (1986) 477–481.

[18] K.N. Volkov, V.N. Emelyanov, A.V. Pustovalov, Supersonic flows of an inviscid compressible gas in aerodynamic windows of gas lasers, Numerical Methods and Programming 15 (2014) 712–725.

[19] V.N. Emelyanov, A.V. Pustovalov, K.N. Volkov, Supersonic jet and nozzle flows in uniform-flow and free-vortex aerodynamic windows of gas lasers, Acta Astronautica 163 (2019) 232–243.

[20] G. Rudinger, Fundamentals of gas particle-flow, Amsterdam–Oxford–New York, Elsevier, 1980.

[21] H. Miura, I.I. Glass, Supersonic expansion of a dusty gas around a sharp corner, Proceedings of the Royal Society of London, Series A 415 (1988) 91–105.

[22] Y. Ling, A. Haselbacher, S. Balachandar, Transient phenomena in one-dimensional compressible gasparticle flows, Shock Waves 19 (2009) 67–81.

[23] Q.-S. Wu, H. Zhu, Y.-H. Xu, B.Y. Wang, Numerical study of shock diffraction in dusty gases, Applied Mathematics and Mechanics 16 (1995) 79–85.

[24] Z.-X. Ren, B. Wang, H. Zhang, Fast numerical solutions of gas-particle two-phase vacuum plumes, Advances in Mechanical Engineering 5 (2013) 765627.

[25] G.V. Molleson, A.L. Stasenko, Acceleration of microparticles in a gas-dynamic installation with a large flow expansion, High Temperature 46 (2008) 110–118.

[26] K.N. Volkov, V.N. Emelyanov, I.V. Teterina, M.S. Yakovchuk, Gas flows in nozzle of energy systems. Moscow, Publishing House of Physical and Mathematical Literature, 2016.

[27] G.V. Molleson, A.L. Stasenko, Gas thermodynamics and optics of a monodisperse jet interacting with a streamlined body, High Temperature 50 (2012) 810–819.

[28] A. Venkattraman, A.A. Alexeenko, Simulations and measurements of gas-droplet flows in supersonic jets expanding into vacuum, AIAA Paper 2009-3751 (2009).

[29] F. Dorchies, F. Blasco, T. Caillaud, J. Stevefelt, C. Stenz, A.S. Boldarev, V.A. Gasilov, Spatial distribution of cluster size and density in supersonic jets as targets for intense laser pulses, Physics Review A68 (2003) 023201.

[30] G. Chen, B. Kim, B. Ahn, D.E. Kim, Determining the mean size and density of clusters, formed in super sonic jets, by Rayleigh scattering and Mach-Zehnder interferometer, Journal of Applied Physics 108 (2010) 064329.

[31] K. Luria, W. Christen, U. Even, Generation and propagation of intense supersonic beams, The Journal of Physical Chemistry A 115 (2011) 73627367.

[32] M. Patel, J. Thomas, H.C. Joshi, Flow characterization of supersonic gas jets: experiments and simulations, Vacuum 192 (2021) 110440.

[33] J.C. Lengrand, V.G. Prikhodko, P.A. Skovorodko, I.V. Yarygin, V.N. Yarygin, Outflow of gas from supersonic nozzle with screen into vacuum, AIP Conference Proceedings 1333 (2011) 583.

[34] V.G. Prikhodko, V.N. Yarygin, I.V. Yarygin, Experimental study of droplet detachment from liquid film surface by a co-current flow inside the nozzle stagnation chamber, Journal of Physics: Conference Series 1677 (2020) 012148.

[35] A.E. Zarvin, K.A. Dubrovin, A.S. Yaskin, V.V. Kalyada, V.E. Khudozhitko, Simulation of the spacecraft supersonic jets in vacuum on small-sized laboratory installations, Journal of Physics: Conference Series 1799 (2021) 012040.

[36] F. Bernard, A. Iollo, G. Puppo, Simulation of particle dynamics for rarefied flows: backflow in thruster plumes, European Journal of Mechanics, B/Fluids 63 (2017) 25–38.

[37] M. Ivanov, A. Kudryavtsev, G. Markelov, P. Vashchenkov, D. Khotyanovsky, A. Schmidt, Numerical study of backflow for nozzle plumes expanding into vacuum, AIAA Paper 2004-2687 (2004).

[38] R. Engeln, S. Mazouffre, P. Vankan, D.C. Schram, N. Sadeghi, Flow dynamics and invasion by background gas of a supersonically expanding thermal plasma, Plasma Sources Science and Technology 10 (2001) 595–605.

[39] S.E. Selezneva, M.I. Boulos, M.C.M. van de Sanden, R. Engeln, D.C. Schram, Stationary supersonic plasma expansion: continuum fluid mechanics versus direct simulation Monte Carlo method, Journal of Physics D: Applied Physics 35 (2002) 1362–1372.

[40] C.B. Henderson, Drag coefficients of spheres in continuum and rarefled flows, AIAA Journal 14 (1976) 707–708.

[41] A.V. Struchkov, A.S. Kozelkov, K.N. Volkov, A.A. Kurkin, R.N. Zhuckov, A.V. Sarazov, Numerical simulation of aerodynamic problems based on adaptive mesh refinement method, Acta Astronautica 172 (2020) 7–15.

[42] K. Volkov, Multigrid and preconditioning techniques in CFD applications, in: Z. Driss, B. Necib, H.-C. Zhang (Eds.), CFD Techniques and Thermo-Mechanics Applications, Springer International Publishing, 2018, pp. 83–149.